THE JOURNAL OF PHYSICAL CHEMISTRY C

Article

Cite This: J. Phys. Chem. C 2019, 123, 19820−19827

pubs.acs.org/JPCC

Edge Doping Effect to the Surface Plasmon Resonances in Graphene Nanoribbons

Don C. Abeysinghe,[†] Nima Nader,[‡,§,▽] Joshua Myers,[†,∥,▽] Joshua R. Hendrickson,[§] Justin W. Cleary,[§] Dennis E. Walker, Jr.,[§] Kuei-Hsien Chen,[⊥] Yongmin Liu,[#] and Shin Mou*[,†]

[†]Materials & Manufacturing Directorate, Air Force Research Laboratory, Wright-Patterson AFB, Ohio 45433, United States

[‡]Solid State Scientific Corporation, Nashua, New Hampshire 03060, United States

[§]Air Force Research Laboratory, Sensors Directorate, Wright-Patterson AFB, Ohio 45433, United States

[∥]Department of Electrical Engineering, Wright State University, Dayton, Ohio 45435, United States

[⊥]Institute of Atomic and Molecular Sciences, Academia Sinica, Taipei 106, Taiwan

[#]Department of Mechanical and Industrial Engineering, Department of Electrical and Computer Engineering, Northeastern University, Boston, Massachusetts 02115, United States

Supporting Information

ABSTRACT: In this work, we investigated the edge doping effect to graphene plasmon resonances in graphene nanoribbons (GNRs), which is known to affect the electronic doping of GNRs but has not been systematically studied. We found the Fermi levels, which reflect that the sheet charge carrier densities, extracted from the graphene plasmon resonance frequencies, vary across GNRs of different widths on the same sample. Using Raman spectroscopy, we confirmed that the variation of the sheet charge carrier density is caused by edge doping, which has a stronger effect on narrower GNRs. To further understand the edge doping effect, electron beam irradiation (EBI) is applied to modify the charge state of the edge. Using EBI, we successfully demonstrated the tuning of the graphene plasmon resonances due to the change of the edge doping states. These findings demonstrated the importance of the edge doping effect in determination of the surface plasmon frequency in GNRs.

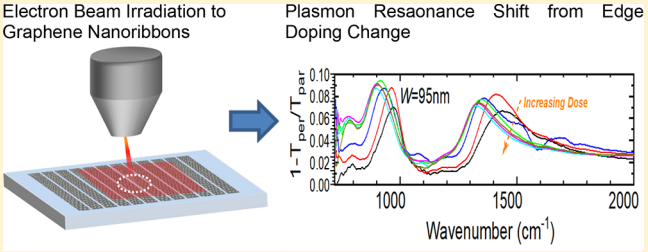

INTRODUCTION

Graphene, a single atom sheet of sp^2-bound carbon, is a semimetal with high carrier mobility and high conductivity.[1−3] Due to the abundant free carriers, the collective charge carrier oscillations, the so-called surface plasmons, can be excited in graphene micro- or nano-structures. It has been demonstrated that graphene nanoribbons (GNRs) on the order of 100 nm or narrower can support plasmon resonances in the mid-infrared (mid-IR) range.[4−7] Since mid-IR is an important wavelength region for various applications including infrared sensing,[8,9] infrared polarization conversion,[10] plasmonically induced transparency,[11] chemical and biological sensing,[12] and beam steering,[13−15] researchers have been exploring the utilities of graphene plasmons in these areas.

It is understood that the surface plasmon resonance frequency in GNRs is a function of the width and the carrier density of the ribbons,[16] both of which can be affected by the edge effects when the dimension of the graphene structure is at the nanoscale. It is postulated by Yan et al.[4] that an "inactive" area on the edge of the GNRs about 28 nm wide reduces the width of the effective area in which the plasmons oscillate. The inactive edge, albeit difficult to characterize at the nanoscale, has been evidenced by Raman spectroscopy[17] and microwave atomic force microscopy[18,19] to show different characteristics than in the basal plane. In addition to that, Fei and Rodin et al. also alluded that in exfoliated graphene, the carrier density is enhanced near the sample edge by using near-field infrared nanoimaging.[7] With the same technique applied to lithographically patterned chemical vapor deposition (CVD) GNRs, Fei and Goldflam et al.[20] found that the patterned graphene edges have profound effects of doping, scattering, and plasmon reflection, which are presumably caused by edge defects and roughness. Brar et al.[6] suggested that "edge states can be introduced on GNRs as a result of the lithography, and that can lead to a constant change in the background charge density for GNRs". Finally, Brenner et al.[21] demonstrated that graphene edges are efficient doping centers through the passivation and functionalization of the edges. This so-called edge doping effect was observed by several groups mentioned above. However, it has not been studied systematically in regard to the change it induces on the surface plasmon resonance frequency. Moreover, this is a practically important

Received: April 17, 2019
Revised: July 12, 2019
Published: July 17, 2019

DOI: 10.1021/acs.jpcc.9b03635
J. Phys. Chem. C 2019, 123, 19820−19827

issue since the shift and the inhomogeneous broadening of the plasmon resonance frequency caused by the edge doping variation can be detrimental for applications such as infrared detection,[9] beam steering,[13−15] and chemical/biological sensing[12] relying on surface plasmon resonances in GNRs. Therefore, it is critical to understand the edge doping and its potential effects on these applications.

To this end, we studied the surface plasmon dispersion in GNRs to understand the edge doping effect and how it may change the overall doping level in GNRs. Raman spectroscopy was used to characterize the doping change as a function of the nanoribbon width. In addition, we use electron beam irradiation (EBI) to modify the edge states of the GNRs and to tune the surface plasmon resonances. We purposely applied low-energy (~10 kV) and low-dose (20 μC/cm^2 maximum) electron irradiations to minimize the damage to the basal plane graphene lattices. This resulted in the tuning of graphene plasmon resonances with red shifts as the electron beam dose step increases, which is consistent with the reduction of the carrier densities in GNRs. Based on Raman spectroscopy, we confirmed that the reduction of carrier densities resulted most likely from the interaction of the EBI with the GNR edges. Our research findings shed new light on the edge effect of GNRs and open up opportunities to design tunable plasmonic and optoelectronic devices in the crucial mid-IR regime.

EXPERIMENTAL SECTION

Sample Preparation. In our experiments, graphene was grown on 25 μm-thick copper foils using the CVD method.[22] After the transfer of graphene onto SiO_2-on-Si wafers, GNR arrays were patterned using an electron beam lithography system with a 100 kV electron beam. Graphene was then etched and defined using oxygen plasma reactive ion etching. Using this process, we were able to fabricate GNRs over 200 by 200 μm^2 areas with their widths varying from 215 to 55 nm. The substrate for all of our samples was 290 nm-thick SiO_2 on top of phosphorus-doped n-type silicon wafers with a resistivity in the range of 1−30 Ω cm. Hall measurement of transferred graphene samples from the same batch of the materials of GNRs confirmed a p-type carrier density of around 2 × 10^{13} cm^{-2} and mobility values around 1000 cm^2 V^{-1} s^{-1}. To measure the transmission spectra of the GNR arrays, we used a Bruker Vortex 80V Fourier transform infrared spectrometer (FTIR) with an attached infrared microscope. The incident infrared light was polarized by a CaF_2 wire grid polarizer. The infrared beam spot size on the GNRs was approximately 50 × 50 μm^2, significantly smaller than the area of the arrays (200 × 200 μm^2). Infrared transmission spectra from 700 to 3000 cm^{-1} were collected for GNRs of varying widths of W ~55, 75, 95, 135, 165, 215 nm, as determined by visual inspection with a scanning electron microscope (SEM).

Electron Beam Irradiation. In the electron beam irradiation experiments, single-layer graphene sheets (SLGSs), as well as GNRs, were irradiated with electron beams in the Tescan LYRA-3 (Model XMH I) SEM system, which allowed for accurate control of the exposed area and the electron beam dose. For all experiments, we used an electron beam accelerating voltage of 15 kV, a working distance of 6 mm, a beam current of 300 pA measured with a Faraday cup, and an exposed area of 200 × 200 μm^2.

RESULTS AND DISCUSSION

Infrared Spectroscopy of Plasmon Resonances in Graphene Nanoribbons. Figure 1a shows a schematic of a GNR sample on a SiO_2/Si substrate and the definition of field polarization for the incident light. Distinct polarization dependence of the infrared spectroscopy of GNRs is shown in Figure 1b, where the spectra corresponding to perpendicular (parallel) polarization with respect to the long axis of GNRs are plotted in black (red). Here, three major resonance peaks are identified within our measurement frequency range of 700−3000 cm^{-1} for perpendicular polarization, which are associated with the plasmon resonances. On the other hand, parallel polarization shows free carrier absorption only at the long-wavelength end. Therefore, a figure of merit for absorption was calculated from the transmission spectrum defined as $1 - T_{per}/T_{par}$, where T_{per} and T_{par} are transmittances for the polarization perpendicular and parallel to the GNRs, respectively. Figure 1c shows the transmission spectra ($1 - T_{per}/T_{par}$) for GNRs with their width W ranging from 55 to 215 nm (50% duty cycle). Here, the three major resonance peaks are marked as 1, 2, and 3. Peaks 1 and 2 are known as the hybridized modes and also called surface plasmon phonon polaritons (SPPPs), while peak 3 corresponds to the graphene plasmon (GP) mode.[6] As shown in Figure 1c, all resonance peaks blue-shift as W decreases albeit at significantly different rates. In particular, the peak marked three disperses at a much faster rate as a function of the wavenumber. Moreover, while the line widths of peaks 1 and 2 remain almost constant, peak 3 broadens as a function of the wavenumber due to the fast damping caused by the graphene intrinsic optical phonon at 1580 cm^{-1} (shown in the vertical dashed line in Figure 1c).

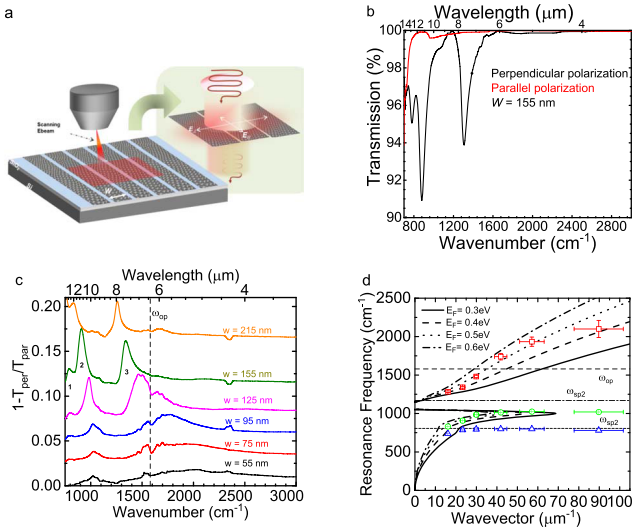

Figure 1. Plasmonic resonant absorption experiment on GNRs. (a) Schematic of the GNR sample and the experiment: the left-hand side shows the electron beam irradiation experiment and the right-hand side illustrates the optical transmission measurement. (b) Transmission spectra for an array of GNRs (W = 155 nm) on SiO_2 with the incident light polarization parallel (red) and perpendicular (black) to the ribbons, respectively. (c) Experimental transmission spectra ($1 - T_{per}/T_{par}$) of GNRs on SiO_2 substrate for varying GNR widths; spectra are offset for clarity. (d) Experimentally extracted graphene plasmon dispersion curves (data points) along with the calculated dispersion curves (black lines).

DOI: 10.1021/acs.jpcc.9b03635
J. Phys. Chem. C 2019, 123, 19820−19827

These observations agree well with the previously reported work on graphene plasmon resonances in the mid-IR.[4,6]

In Figure 1d, we plot the dispersion curves of the resonance frequency against wavevector for the three peaks (see the Supporting Information for the construction of the plot). It clearly shows that the SPPP modes are coupled with the SiO_2 surface phonon modes at ω_{sp1} = 806 cm^{-1} and ω_{sp2} = 1168 cm^{-1}, where the anticrossings occur at around these two frequencies. The slow dispersion of the phonon-like modes, the peak 1 and peak 2, can be explained by their positions in close proximity to ω_{sp1} and ω_{sp2}, respectively. The fast dispersion of the graphene plasmon mode, the peak 3, approximately follows the well-established relation $\omega_p \propto \sqrt{q}$, where q is the wavevector.[16] Using an analytical equation (see the Supporting Information), we plot the dispersion curves (black curves) with Fermi energy E_F varying from 0.3, 0.4, 0.5 to 0.6 eV. While the analytical curves fit the experimental data reasonably well, it is difficult to have a perfect fit using a single Fermi energy. In addition, we need to subtract 20 nm off the physical ribbon width to derive an effective width due to the defective area along the edges caused by the harsh reactive ion etching.[4] The interesting observation is that for the wider ribbons (W > 100 nm) the Fermi level stays closer to 0.4 eV, and for the narrower ribbons (W < 100 nm), the Fermi level increases toward 0.5 eV. As pointed out by Peres et al.,[23] the narrower the nanoribbons are, the heavier the edge doping is contributing to the overall doping level. Therefore, we hypothesize that the Fermi level shift is mainly caused by the edge doping effect, which is a function of the nanoribbon width and the dry-etching condition. To verify our theory, we turn to Raman spectroscopy, which is a common technique to characterize doping in carbon-based materials.

Raman Spectroscopy of Graphene Nanoribbons. Raman spectroscopy is a fast and nondestructive characterization method in revealing intrinsic phonon vibrational properties and chemical bond structures of various carbon materials.[24,25] Raman spectroscopy is known to characterize microscopic information such as the amount of disorder,[26] doping,[27,28] and chemical modification,[29] as well as the atomic arrangements at the edges.[30,31] The Raman spectrum of graphene consists of a set of distinct peaks in the 800−3000 cm^{-1} region: the G and D peaks, around 1582 and 1350 cm^{-1}, respectively, as well as the second-order peak 2D at 2690 cm^{-1} (also referred to the G′ peak). The G peak corresponds to the E_{2g} phonon at the Brillouin zone center known as the Γ point. The D peak is due to the breathing modes of six-atom rings and requires a defect for its activation.[32,33] The 2D peak originates from a second-order, double-resonant Raman scattering mechanism.[27,29,33,34]

It has been reported that the characteristic Raman G and 2D peaks are sensitive to the presence of doping,[35,26] where p-type doping corresponds to the upshifting of both G and 2D bands, while n-type doping corresponds to an opposite shifting in G and 2D modes.[35] In addition, other works[27,35] have shown that the intensity ratio of $I(2D)/I(G)$ is a sensitive parameter to estimate the doping density. To summarize the trend, in continuous SLGSs, the height (or area) ratio of the 2D and G peaks, $I(2D)/I(G)$ (or $A(2D)/A(G)$), is at a maximum for zero doping and decreases for increasing doping for both n-type and p-type dopings[24] (see eq 1). Applying the Raman spectroscopy analysis on GNRs, we observed that as one moves from the SLGS to narrow GNRs, the spectral weight shifts from the 2D band to the G band and D band in Figure 2a. In Figure 2b, we have summarized the spectra in Figure 2a, demonstrating that $I(D)/I(G)$ increases rapidly as the width of

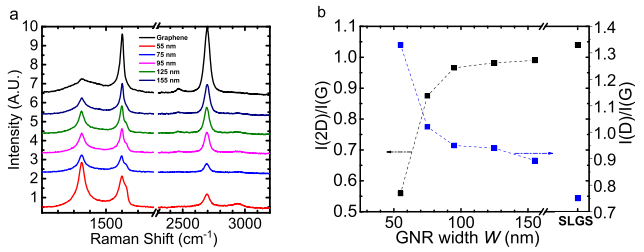

Figure 2. Raman spectra of GNRs in comparison with that of an unpatterned SLGS: (a) Raman spectra for GNRs of various widths and a SLGS for a 532.3 nm wavelength laser excitation and (b) plot of $I(2D)/I(G)$ and $I(D)/I(G)$ for GNRs of various widths in comparison with an SLGS.

the GNR narrows down and the $I(2D)/I(G)$ trends in the opposite direction. For the wider GNRs in this figure, with widths larger than 100 nm, the values of $I(D)/I(G)$ and $I(2D)/I(G)$ are comparable to those of the SLGS. Therefore, we conclude that the increase of $I(D)/I(G)$ is due to defects and disorders on the GNR edges because of the dangling bonds and the edge functional groups caused by plasma etching. Based on a previous near-field optical and micro-Raman studies by Fei et al.,[7] we know higher doping happens at around the graphene edge, which explains the reduction of $I(2D)/I(G)$ toward narrower GNR widths. In short, the defects and disorders generated at the edges of the GNRs become the dopants for GNRs to increase the overall doping level. As the edge carbon atoms represent a larger fraction of the total carbon atoms for narrower GNRs, their doping levels deviate more from that of the SLGS. This is consistent with previous reports.[17,36,37] Besides the natural edge-dangling bonds, we would like to point out that our GNRs were patterned using oxygen plasma, a harsh oxidizing condition, which is known to form various oxygen-containing functional groups on graphite[36,38,39] that is electronegative and expected to withdraw π-electrons of GNRs, i.e., acting as acceptors. Certainly, Brenner et al. demonstrated that oxygen-terminated zig-zag graphene edges are efficient p-type doping sources, which donate 0.85 hole per edge carbon atom.[21] Since our SLGS was p-type, as originally confirmed by Hall effect measurements, the edge doping should cause increased p-type doping to the GNRs compared to that of the SLGS, consistent with the observation in the Raman spectroscopy.

An empirical equation developed in Casiraghi et al.[40] describing $I(2D)/I(G)$ dependence on graphene Fermi energy level can be used to further explain the observed Raman shifts. The equation is given as

$$\sqrt{I(2D)/I(G)} = 1/C'(\gamma_{ep} + 0.07|E_F|) \quad (1)$$

where C' is a constant and γ_{ep} is the scattering rate for carriers in graphene by phonons. This equation, plotted in Figure 3, shows that GNRs have significantly lower values of $I(2D)/I(G)$ than SLGS, which means they are more deeply p-type-doped than the SLGS. The doping type of the SLGS and the GNRs were confirmed to be p-type by the Hall effect measurement and field-effect transistor transconductance measurement, respectively, which are consistent with previous reports.[6,16] Using the previously estimated experimental value $\gamma_{ep} \sim 20$ meV, we obtain E_F = −0.484 and −0.291 eV for 55

DOI: 10.1021/acs.jpcc.9b03635
J. Phys. Chem. C 2019, 123, 19820−19827

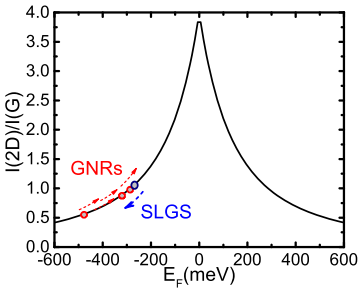

Figure 3. Plot of $I(2D)/I(G)$ as a function of the Fermi energy based on eq 1. The unfilled circles insert the $I(2D)/I(G)$ data points of the GNRs (red) and SLGS (blue) from Figure 2b (before EBI) along the curve. The positive (negative) Fermi energy corresponds to n-type (p-type) doping. This plot clearly shows that the GNRs are more heavily p-type-doped than the SLGS and also the GNRs become more p-type as their widths are narrower. The arrows indicate the $I(2D)/I(G)$ shift after EBI directionally. The SLGS (blue arrow) becomes more heavily p-type-doped but the GNRs (red arrows) become less p-type-doped.

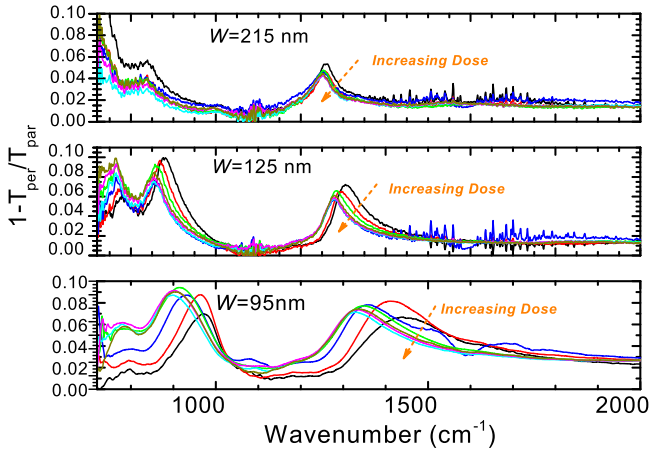

Figure 4. Tuning of graphene plasmon spectra by EBI for three representative GNRs with widths W = 95, 125, and 215 nm.

and 155 nm wide GNRs, respectively. Qualitatively, this is consistent with our observation from the plasmon resonance dispersion (Figure 1d), in which narrower GNRs tend to have higher Fermi levels. Raman spectroscopy confirms our hypothesis that the Fermi level of graphene is not a constant when they are etched into narrow GNRs because the edge doping becomes comparable to the surface doping at this scale.

Electron Beam Irradiation of Graphene Nanoribbons. To further demonstrate the importance of the edge doping, we conduct an experiment in which we modify the GNR edge doping and cause the tuning of plasmon resonances upon EBI. The samples under investigation are the same set of GNR array samples used for the results in Figure 1. Previously, researchers[41,42] showed that the EBI is an effective tool for generating and manipulating defects in graphene and other carbon-based materials. We note that, unlike in previous EBI studies on graphene[41,42] where a large amount of defects were generated, here we purposefully use low-energy (<15 kV), low-dose (<25 μC/cm^2) EBI conditions to avoid weakening of the electronic nature of the sp^2 covalent bonds in graphene to minimize additional defect generation. In other words, we attempt to only affect the edge defects of GNRs but not generate additional defects in the center of the GNRs. Upon EBI, Figure 4 clearly shows red-shifting of the graphene plasmon spectra for three representative GNRs of different widths (95, 125, and 215 nm) with a step increase in EBI dose levels. Figure 5a shows that the resonance shifts for both SPPP and GP modes reached saturation at the same EBI dose value of $\sim 15 \times (2.25 \times 10^{-1}$ μC/cm^2). This indicates that the tuning mechanism is likely related to impurities, traps, and defects, which have a limited density. On the other hand, we estimated the plasmon oscillator strength by integrating the summed areas over peaks 1, 2, and 3 in the spectra in Figure 4. The result in Figure 5b shows ~3% increment of the SPPP oscillation strength from 0 dose to maximal EBI dose at 22.5 μC/cm^2. This suggests that the electronic quality of graphene is not degraded. These two observations are consistent with the hypothesis that the EBI modified the defects at the GNR edges but did not create extra defects in the bulk of the graphene, which generally degrades the electronic properties.

To further evaluate the effect of the EBI, we show the correlation between the plasmon resonance frequency and the plasmon scattering rate over incrementally accumulated EBI dose in Figure 5c. Note that the plasmon scattering rate calculated here uses a Fano resonance model similar to the model used in Yan et al.[4] The total plasmon scattering rate, which is derived from the fitting using the Fano resonance model (see the Supporting Information), is the sum of the rates of several scattering mechanisms including GNR edge scattering, scattering with the SiO_2 surface phonon modes, scattering with the intrinsic graphene phonon, and impurity scattering. While it is probable that charge exchange between graphene and the environment happens during the EBI, which, in all likelihood, induces more charged impurity centers for scattering, the total plasmon damping rate decreases as a function of the EBI dose. The implication is that the GNR plasmon damping in the mid-IR is not dominated by charged impurity scattering, which is consistent with the observation in Yan et al.,[4] in which they concluded that the GNR plasmon damping in the mid-IR was dominated by edge scattering, graphene optical phonon scattering, and the hybridization with the SiO_2 surface phonon modes. However, the reduction of the plasmon scattering rate proves that our EBI is not detrimental to the plasmon resonances, due to the low electron dose/energy level. Dispersion curves are useful in determining the doping level in GNRs; we plotted them based on the Kubo formula[43] and matched them with experimental data in Figure 5d (see the Supporting Information). Best matching plasmon dispersion curves with experimental data for before and after the maximum EBI dose give $\Delta E_F \simeq 0.1$ eV; this corresponds to the original Fermi energy level for our graphene samples to be ~ -0.5 and -0.4 eV after the EBI. To further verify the results, we use Raman spectroscopy again to understand the defect modification and the doping caused by the EBI.

Recall that in the previous section we used the ratios of $I(D)/I(G)$ and $I(2D)/(G)$ to explain the edge doping in GNRs. In this section, we attempt to use these ratios to explain the effect of the EBI on the GNR edges. Figure 6a,b shows Raman spectra for an SLGS and for a set of 100 nm wide GNRs, respectively, for various EBI doses. Figure 6c summarizes the data in Figure 6a,b and indicates that $I(2D)/I(G)$ has a clear dependence on the EBI dose amount. For the GNRs, the increase of $I(2D)/I(G)$ corresponds to the reduction of carrier density (see Figure 3), which is consistent with the red shift in graphene plasmon resonance measurements. Also, note that $I(2D)/I(G)$ reached a saturation for an EBI dose value of around $15 \times 2.25 \times 10^{-1}$ μC/cm^2 for both

DOI: 10.1021/acs.jpcc.9b03635
J. Phys. Chem. C 2019, 123, 19820−19827

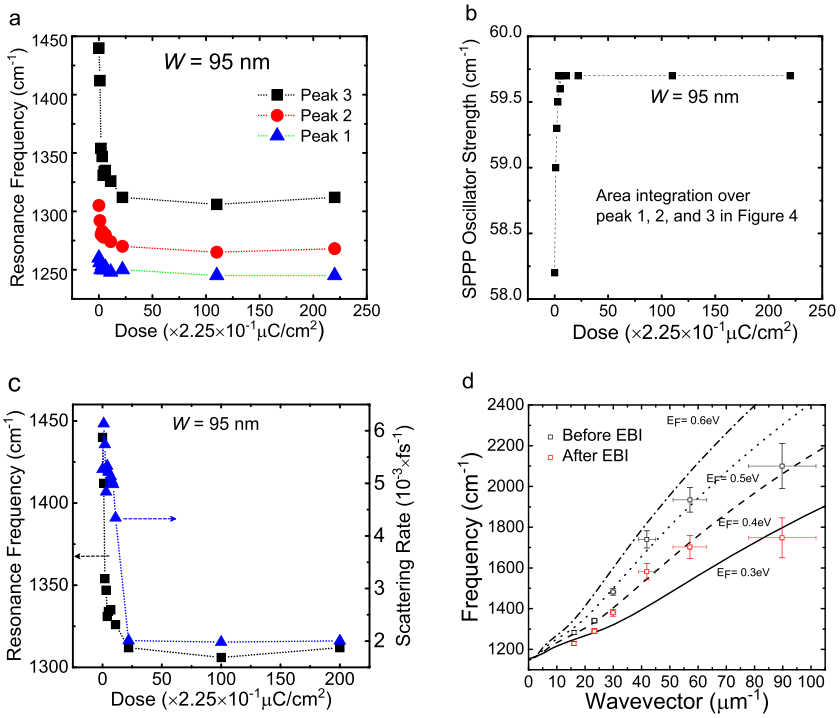

Figure 5. (a) Resonance frequency variation for the GNRs of W = 95 with EBI for peaks 1, 2, and 3, as indicated in Figure 4; (b) resonance frequency and total scattering rate for plasmons with respect to increasing EBI for the same GNRs; (c) variation of plasmon oscillator strength with EBI, calculated by integrating the area under peaks 1, 2, and 3 for GNRs with W = 95 nm; and (d) experimental data plotted with simulated plasmon dispersion curves for various Fermi energy levels.

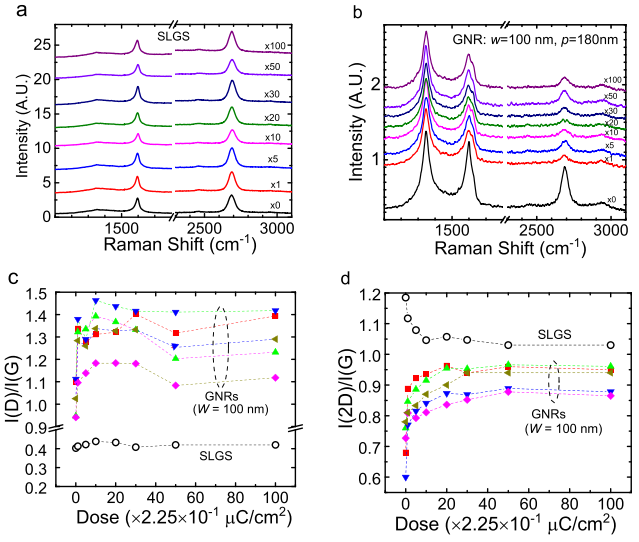

Figure 6. Raman characterization of GNRs in comparison to that of the SLGS upon various doses of EBI: the evolution of the Raman spectra with increasing EBI dose factors for (a) SLGS and for (b) a representative case of several GNRs of width W = 100 nm and period p = 180 nm. The spectra are offset for clarity. (c) Plot of Raman $I(2D)/I(G)$ versus EBI for GNRs and the SLGS. A dose factor of 100 is equivalent to a value of 22.5 μC/cm^2. (d) Raman $I(D)/I(G)$ for the SLGS and five GNR samples of width W = 100 nm and period p = 180 nm for varied dose values.

the SLGS and GNRs; a similar saturation behavior could be observed earlier in Figure 5a,b in the plasmon resonance absorption spectra and in the scattering rate data where saturation was reached at approximately the same EBI dose value of 15 × 2.25 × 10^{-1} μC/cm^2.

Interestingly, the variation of $I(2D)/I(G)$ as a function of the EBI dose amount with respect to the GNRs and the SLGS film shows mirror-opposite trends. We illustrate this fact in Figure 3, in which the red arrows represent increased $I(2D)/I(G)$ numbers of GNRs upon the EBI, and the blue arrow shows a decreased $I(2D)/I(G)$ number of the SLGS upon the EBI. This shows fundamentally different doping behaviors in the SLGS and GNRs. Based on eq 1 and Figure 3, we conclude that the doping concentration of the GNRs reduces on the orders of 10^{12}−10^{13} cm^{-2} and the doping concentration of the SLGS increases to about 10^{13} cm^{-2} for the maximal EBI dose. To understand what that means and whether it is related to the modification of the edge states, we examine the possible mechanisms to cause the red shift of graphene plasmon resonances and the Raman spectroscopy upon the EBI. The first possible cause is from the charging of the surface trap states of the SiO_2 substrate. Previous EBI studies on bulk graphene have demonstrated EBI-induced filling of surface trap states of SiO_2 substrate and the resulting trapped charge density change on SiO_2, which generates additional doping to graphene.[44,45] Burson et al.[44] demonstrated that SiO_2 substrates can reach a metastable state 8 h after electron beam doping with a charged impurity density of ∼2 × 10^{11} cm^{-2}. While the charging of SiO_2 surface trap states is a factor here, these relatively large doping concentration changes cannot be simply explained by that since the reported metastable charge density in SiO_2 after the EBI is at least an order of magnitude smaller than the charge density observed. Second, it is well known that amorphous carbon deposition can happen during the EBI due to the existence of environmental carbon sources. This effect may result in charge exchanges and/or modification of the dielectric environment, i.e., from air to amorphous carbon, which are possible to red-

DOI: 10.1021/acs.jpcc.9b03635
J. Phys. Chem. C 2019, 123, 19820−19827

shift the plasmon resonances. Typically, the Raman signature of amorphous carbon is a broad G peak, as well as a strong D peak.[32] In Figure 6a of the Raman spectra from the SLGS with various EBI doses, we do not observe broadening of the G band and increase of the D band intensity. Therefore, we believe that the effect of amorphous carbon deposition is minimal.

Defect generation and modification along the edges of GNRs using the EBI are the objective of the study here. Dangling bonds and functionalized sites at the edge of the GNRs are likely to have a weaker bond strength, which is more likely to be affected by the EBI compared to the carbon sp^2 bonds. For defect information in carbon materials, the $I(D)/I(G)$ ratio is the most common parameter to measure this effect, which is plotted in Figure 6c. Like we expected, the $I(D)/I(G)$ of the SLGS is mostly unchanged as a function of the EBI dose, which means that defect generation in the SLGS upon the EBI is negligible. This is what we expected when we chose to use low-energy and low-dose EBI. However, the $I(D)/I(G)$ ratio of the GNRs trends upward as a function of the EBI dose and saturates around $15 \times 2.25 \times 10^{-1}$ $\mu C/cm^2$, which is different from the case of the SLGS. Therefore, we can conclude that the doping change, which causes the red shift in graphene plasmon resonances, results from the defect generation/modification upon the EBI in the GNRs. A probable explanation is that the EBI knocked off the edge oxygen functional groups, which then causes edge carbons to reconstruct or bond with other atoms (e.g., hydrogen) to reduce the p-type doping.[21] This explanation naturally answers the discrepancy between the GNRs and the SLGS upon the EBI. Since our electron energy is well below the knock-on energy of the carbon sp^2 bonds, it is very likely that the EBI only modified the GNR edge defects/functional sites but did not affect the bonds of the graphene basal plane. We hypothesize that the doping change in SLGS is due to an environmental effect, which means that the EBI causes charge exchanges between the environment (e.g., residual surface polymers and the substrate) and the SLGS. The above results and discussion suggest that edge doping can be an effective way to modulate the doping density in GNRs in addition to the top surface doping. Based on our findings, edge doping does not further dampen the plasmon resonances in GNRs and can change the carrier density and the plasmon frequency of GNRs substantially. More importantly, chemisorbed functional groups can be applied to the edge-dangling bonds without further damaging the bonding structure of the graphene sp^2 bonds, which can be useful in both doping and passivating GNRs.[21]

CONCLUSIONS

In summary, with the combination of infrared spectroscopy and Raman spectroscopy, we explained that the edge doping of GNRs can affect the overall doping and carrier density in GNRs. The shift of the Fermi level created by edge doping is affected by the GNR width and the etching process condition. Moreover, we demonstrated that the surface plasmon frequency of GNRs can be tuned in a controlled manner by introducing electrical charges through low-energy, low-dose EBI. The results show that the plasmon frequency red shift is tuned by the defect modification along the edges of the GNRs by the EBI. Raman spectroscopy confirms that result with the increase of both $I(D)/I(G)$ and $I(2D)/I(G)$ ratios, which means the doping density increases as the defect/disorder density increases. On the other hand, the pristine SLGS shows a minimal generation of defects/disorders upon the EBI for the same energy and dose values. This is due to the fact that the existing dangling bonds and defects at the edges are more reactive than the carbon sp_2 bonds so that they are prone to the change in their charge states upon the irradiation of the electron beam. This suggests that edge doping and functionalization are useful with regard to graphene plasmons in GNRs for applications such as infrared sensing and chemical and biological sensing.

ASSOCIATED CONTENT

Supporting Information

The Supporting Information is available free of charge on the ACS Publications website at DOI: 10.1021/acs.jpcc.9b03635.

Extraction of the plasmon damping rate from the experimental transmission spectra; Fano fitting for the plasmon mode for a 95 nm wide GNR for different EBI dose factors (Figure S1); and derived results using Fano resonance fitting (Table S1) (PDF)

AUTHOR INFORMATION

Corresponding Author

*E-mail: shin.mou.1@us.af.mil.

ORCID

Joshua R. Hendrickson: 0000-0002-5342-0346

Shin Mou: 0000-0001-5228-2562

Present Address

[∇]Applied Physics Division, National Institute of Standards and Technology, 325 Broadway, Boulder, Colorado 80305, United States (N.N.), Altamira Technology Corporation, 2850 Presidential Dr. #200, Fairborn, Ohio 45324, United States (J.M.).

Author Contributions

S.M. supervised this research. D.C.A. contributed to graphene structure fabrication, FTIR measurements, Raman spectroscopy measurement, and electron beam irradiation. J.M. contributed to graphene transfer and graphene structure fabrication. J.R.H., J.W.C., and N.N. contributed to FTIR measurements. D.E.W. contributed to graphene structure fabrication. K.-H.C. contributed to graphene synthesis. Y.L. contributed to the calculations of plasmon damping rate and plasmon dispersion curve. The manuscript was written through contributions of all authors. All authors have given approval to the final version of the manuscript.

Notes

The authors declare no competing financial interest.

ACKNOWLEDGMENTS

S.M., D.C.A., and J.M. acknowledge the support by the Air Force Office of Scientific Research under award number FA9550-14RX12COR. J.R.H., J.W.C., and N.N. acknowledge the support by the Air Force Office of Scientific Research under award number FA9550-15RYCOR159. H.C. acknowledges the support by the Asian Office of Aerospace Research and Development under award number 15IOA116. Y.L. acknowledges the support of the US Air Force Summer Faculty Fellowship Program and Office of Naval Research under Grant N00014-16-1-2409. The authors would like to thank Adam T. Neal for valuable discussions and Gerrald Landis for experimental assistance.

DOI: 10.1021/acs.jpcc.9b03635
J. Phys. Chem. C 2019, 123, 19820−19827

■ ABBREVIATIONS

GNR, graphene nanoribbon; SLGS, single-layer graphene sheet; EBI, electron beam irradiation; mid-IR, mid-infrared; FTIR, Fourier transform spectrometer; GP, graphene plasmon; SPPP, surface plasmon phonon polariton; CVD, chemical vapor deposition

■ REFERENCES

(1) Geim, A. K.; Novoselov, K. S. The Rise of Graphene. *Nat. Mater.* **2007**, *6*, 183−191.

(2) Castro Neto, A. H.; Guinea, F.; Peres, N. M. R.; Novoselov, K. S.; Geim, A. K. The Electronic Properties of Graphene. *Rev. Mod. Phys.* **2009**, *81*, 109−162.

(3) Nomura, K.; MacDonald, A. H. Quantum Transport of Massless Dirac Fermions. *Phys. Rev. Lett.* **2007**, *98*, No. 076602.

(4) Yan, H.; Low, T.; Zhu, W.; Wu, Y.; Freitag, M.; Li, X.; Guinea, F.; Avouris, P.; Xia, F. Damping Pathways of Mid-Infrared Plasmons. *Nat. Photonics* **2013**, *7*, 394−399.

(5) Abeysinghe, D. C.; Myers, J.; Nader, N.; Hendrickson, J. R.; Cleary, J. W.; Walker, J. D. E.; Chen, K.-H.; Chen, L.-C.; Mou, S. In *Quantum Sensing and Nanophotonic Devices XI*;Razeghi, M., Tournie, E., Brown, G. J., Eds.; Proceedings of SPIE 8993; SPIE: San Francisco, CA, Feb 2−6, 2014.

(6) Brar, V. W.; Jang, M. S.; Sherrott, M.; Lopez, J. J.; Atwater, H. A. Highly Confined Tunable Mid-Infrared Plasmonics in Graphene Nanoresonators. *Nano Lett.* **2013**, *13*, 2541−2547.

(7) Fei, Z.; Rodin, A. S.; Andreev, G. O.; Bao, W.; McLeod, A. S.; Wagner, M.; Zhang, L. M.; Zhao, Z.; Thiemens, M.; Dominguez, G.; et al. Gate-Tuning of Graphene Plasmons Revealed by Infrared Nanoimaging. *Nature* **2012**, *487*, 82−85.

(8) Li, Z.; Lui, C. H.; Cappelluti, E.; Benfatto, L.; Mak, K. F.; Carr, G. L.; Shan, J.; Heinz, T. F. Structure-Dependent Fano Resonances in the Infrared Spectra of Phonons in Few-Layer Graphene. *Phys. Rev. Lett.* **2012**, *108*, No. 156801.

(9) Guo, Q.; Yu, R.; Li, C.; Yuan, S.; Deng, B.; Javier García de Abajo, F.; Xia, F. Efficient Electrical Detection of Mid-Infrared Graphene Plasmons at Room Temperature. *Nat. Mater.* **2018**, *17*, 986−992.

(10) Cheng, H.; Chen, S.; Yu, P.; Li, J.; Den, L.; Tian, J. Mid-Infrared Tunable Optical Polarization Converter Composed of Asymmetric Graphene Nanocrosses. *Opt. Lett.* **2013**, *38*, 1567−1569.

(11) Cheng, H.; Chen, S.; Yu, P.; Duan, X.; Xie, B.; Tian, J. Dynamically Tunable Plasmonically Induced Transparency in Periodically Patterned Graphene Nanostrips. *Appl. Phys. Lett.* **2013**, *103*, No. 203112.

(12) Li, Y.; Yan, H.; Farmer, D. B.; Meng, X.; Zhu, W.; Osgood, R. M.; Heinz, T. F.; Avouris, P. Graphene Plasmon Enhanced Vibrational Sensing of Surface-Adsorbed Layers. *Nano Lett.* **2014**, *14*, 1573−1577.

(13) Carrasco, E.; Tamagnone, M.; Mosig, J. R.; Low, T.; Perruisseau-Carrier, J. Gate-Controlled Mid-Infrared Light Bending with Aperiodic Graphene Nanoribbons Array. *Nanotechnology* **2015**, *26*, No. 134002.

(14) Li, Z. B.; Yao, K.; Xia, F. N.; Shen, S.; Tian, J. G.; Liu, Y. M. Graphene Plasmonic Metasurfaces to Steer Infrared Light. *Sci. Rep.* **2015**, *5*, No. 12423.

(15) Cheng, H.; Chen, S.; Yu, P.; Liu, W.; Li, Z.; Li, J.; Xie, B.; Tian, J. Dynamically Tunable Broadband Infrared Anomalous Refraction Based on Graphene Metasurfaces. *Adv. Opt. Mater.* **2015**, *3*, 1744−1749.

(16) Ju, L.; Geng, B. S.; Horng, J.; Girit, C.; Martin, M.; Hao, Z.; Bechtel, H. A.; Liang, X. G.; Zettl, A.; Shen, Y. R.; et al. Graphene Plasmonics for Tunable Terahertz Metamaterials. *Nat. Nanotechnol.* **2011**, *6*, 630−634.

(17) Bischoff, D.; Güttinger, J.; Dröscher, S.; Ihn, T.; Ensslin, K.; Stampfer, C. Raman Spectroscopy on Etched Graphene Nanoribbons. *J. Appl. Phys.* **2011**, *109*, No. 073710.

(18) Brockdorf, K.; Ji, Z.; Engel, N.; Myers, J.; Mou, S.; Huang, H.; Zhuang, Y. Imaging of Edge Inactive Layer in Micro-Patterned Graphene Monolayer. *Mater. Lett.* **2018**, *211*, 183−186.

(19) Ji, Z.; Myers, J.; Brockdorf, K.; Engel, N.; Mou, S.; Huang, H.; Zhuang, Y. Microwave Imaging of Etching-Induced Surface Impedance Modulation of Graphene Monolayer. *J. Vac. Sci. Technol., A* **2018**, *36*, No. 05G508.

(20) Fei, Z.; Goldflam, M. D.; Wu, J.-S.; Dai, S.; Wagner, M.; McLeod, A. S.; Liu, M. K.; Post, K. W.; Zhu, S.; Jansse, G. C. A. M.; Fogler, M. M.; Basov, D. N. Edge and Surface Plasmons in Graphene Nanoribbons. *Nano Lett.* **2015**, *15*, 8271−8276.

(21) Brenner, K.; Yang, Y.; Murali, R. Edge Doping of Graphene Sheets. *Carbon* **2012**, *50*, 637−645.

(22) Li, X. S.; Magnuson, C. W.; Venugopal, A.; Tromp, R. M.; Hannon, J. B.; Vogel, E. M.; Colombo, L.; Ruoff, R. S. Large Area Graphene Single Crystals Grown by Low Pressure Chemical Vapor Deposition of Methane on Copper. *J. Am. Chem. Soc.* **2011**, *133*, 2816−2819.

(23) Peres, N. M. R.; Guinea, F.; Castro Neto, A. H. Electronic Properties of Disordered Two-Dimensional Carbon. *Phys. Rev. B* **2006**, *73*, No. 125411.

(24) Basko, D. M.; Piscanec, S.; Ferrari, A. C. Electron-Electron Interactions and Doping Dependence of the Two-phonon Raman Intensity in Graphene. *Phys. Rev. B* **2009**, *80*, No. 165413.

(25) Ferrari, A. C.; Robertson, J. Raman Spectroscopy of amorphous, nanostructured, diamond-like carbon, and nanodiamond. *Philos. Trans. R. Soc., A* **2004**, *362*, 2477.

(26) Casiraghi, C.; Pisana, S.; Novoselov, K. S.; Geim, A. K.; Ferrari, A. C. Raman Fingerprint of Charged Impurities in Graphene. *Appl. Phys. Lett.* **2007**, *91*, No. 233108.

(27) Das, A.; Pisana, S.; Chakraborty, B.; Piscanec, S.; Saha, S. K.; Waghmare, U. V.; Novoselov, K. S.; Krishnamurthy, H. R.; Geim, A. K.; Ferrari, A. C.; Sood, A. K. Monitoring Dopants by Raman Scattering in an Electrochemically Top-Gated Graphene Transistor. *Nat. Nanotechnol.* **2008**, *3*, 210−215.

(28) Pisana, S.; Lazzeri, M.; Casiraghi, C.; Novoselov, K.; Geim, A. K.; Ferrari, A. C.; Mauri, F. Breakdown of the Adiabatic Born−Oppenheimer Approximation in Graphene. *Nat. Mater.* **2007**, *6*, 198−201.

(29) Ferrari, A. C.; Meyer, J. C.; Scardaci, V.; Casiraghi, C.; Lazzeri, M.; Mauri, F.; Piscanec, S.; Jiang, D.; Novoselov, K. S.; Roth, S.; Geim, A. K. Raman Spectrum of Graphene and Graphene Layers. *Phys. Rev. Lett.* **2006**, *97*, No. 187401.

(30) Casiraghi, C.; Hartschuh, A.; Qian, H.; Piscanec, S.; Georgi, C.; Fasoli, A.; Novoselov, K. S.; Basko, D. M.; Ferrari, A. C. Raman Spectroscopy of Graphene Edges. *Nano Lett.* **2009**, *9*, 1433.

(31) Basko, D. M. Boundary Problems for Dirac Electrons and Edge-Assisted Raman Scattering in Graphene. *Phys. Rev. B* **2009**, *79*, No. 205428.

(32) Ferrari, A. C.; Robertson, J. Resonant Raman Spectroscopy of Disordered, Amorphous, and Diamondlike Carbon. *Phys. Rev. B* **2001**, *64*, No. 075414.

(33) Thomsen, C.; Reich, S. Double Resonant Raman Scattering in Graphite. *Phys. Rev. Lett.* **2000**, *85*, No. 5214.

(34) Maultzsch, J.; Reich, S.; Thomsen, C. Chirality-Selective Raman Scattering of the D Mode in Carbon Nanotubes. *Phys. Rev. B* **2001**, *64*, No. 121407.

(35) Shi, Y.; Dong, X.; Chen, P.; Wang, J.; Li, L.-J. Effective Doping of Single-Layer Graphene from Underlying SiO2 Substrates. *Phys. Rev. B* **2009**, *79*, No. 115402.

(36) Panchal, V.; Lartsev, A.; Manzin, A.; Yakimova, R.; Tzalenchuk, A.; Kazakova, O. Visualisation of Edge Effects in Side-Gated Graphene Nanodevices. *Sci. Rep.* **2015**, *4*, No. 5881.

(37) Charlier, J.-C.; Eklund, P. C.; Zhu, J.; Ferrari, A. C. In *Carbon Nanotubes*; Jorio, A.; Dresselhaus, G.; Dresselhaus, M. S., Eds.; Springer Berlin Heidelberg: New York, 2008; Vol. *111*, pp 673−709.

(38) Lahiri, J.; Lin, Y.; Bozkurt, P.; Oleynik, I. I.; Batzill, M. An Extended Defect in Graphene as a Metallic Wire. *Nat. Nanotechnol.* **2010**, *5*, 326−329.

DOI: 10.1021/acs.jpcc.9b03635
J. Phys. Chem. C 2019, 123, 19820−19827

(39) Chae, J.; Jung, S.; Woo, S.; Baek, H.; Ha, J.; Song, Y. J.; Son, Y.-W.; Zhitenev, N. B.; Stroscio, J. A.; Kuk, Y. Enhanced Carrier Transport along Edges of Graphene Devices. *Nano Lett.* **2012**, *12*, 1839−1844.
(40) Casiraghi, C. Doping Dependence of the Raman Peaks Intensity of Graphene Close to the Dirac Point. *Phys. Rev. B* **2009**, *80*, No. 233407.
(41) Teweldebrhan, D.; Balandin, A. A. Modification of Graphene Properties due to Electron-Beam Irradiation. *Appl. Phys. Lett.* **2009**, *94*, No. 013101.
(42) Liu, G.; Teweldebrhan, D.; Balandin, A. A. Tuning of Graphene Properties via Controlled Exposure to Electron Beams. *IEEE Trans. Nanotechnol.* **2011**, *10*, 865−870.
(43) Jablan, M.; Buljan, H.; Soljačić, M. Plasmonics in Graphene at Infra-Red Frequencies. *Phys. Rev. B* **2009**, *80*, No. 245435.
(44) Burson, K. M.; Cullen, W. G.; Adam, S.; Dean, C. R.; Watanabe, K.; Taniguchi, T.; Kim, P.; Fuhrer, M. S. Direct Imaging of Carged Impurity Density in Common Graphene Substrates. *Nano Lett.* **2013**, *13*, 3576−3580.
(45) Romero, H. E.; Shen, N.; Joshi, P.; Gutierrez, H. R.; Tadigadapa, S. A.; Sofo, J. O.; Eklund, P. C. n-Type Behavior of Graphene Supported on Si/SiO2 Substrates. *ACS Nano* **2008**, *2*, 2037−2044.

DOI: 10.1021/acs.jpcc.9b03635
J. Phys. Chem. C 2019, 123, 19820−19827